Applied Clay Science 226 (2022) 106572

Contents lists available at ScienceDirect

Applied Clay Science

journal homepage: www.elsevier.com/locate/clay

Synthetic silico-metallic mineral particles SSMMP: A new option for CO_2 capture and CO_2/N_2 separation from post-combustion technology

Daniela Rodrigues [a,c], Franciele Bernard [b], Christophe Le Roux [c], Evandro Duarte [a], Pierre Micoud [c], Alain Castillo [c], François Martin [c], Sandra Einloft [a,b,*]

[a] Post-Graduation Program in Materials Engineering and Technology, Pontifical Catholic University of Rio Grande do Sul – PUCRS, Brazil
[b] School of Technology, Pontifical Catholic University of Rio Grande do Sul PUCRS, Brazil
[c] GET/OMP (CNRS, UT3PS, IRD, CNES), Université de Toulouse, ERT Géomatériaux, Toulouse, France

ARTICLE INFO

Keywords:
Synthetic silico-metallic mineral particles
Synthetic talc
CO_2 sorption
CO_2 selectivity

ABSTRACT

A new class of solid adsorbents based on pristine and ionic liquid (IL) functionalized synthetic silico-metallic mineral particles (SSMMP) for CO_2 capture and CO_2/N_2 separation are presented. Pristine particles were submitted to hydrothermal treatment producing synthetic talc. Samples were characterized by thermal analyses (TGA), specific surface area measurements (BET), infrared spectroscopy (FTIR), Raman spectroscopy, X-ray diffraction(XRD), NMR spectroscopy, and scanning electron microscopy (SEM). Values for specific surface areas varied from 5 m^2/g for a sample with high IL content to 354 m^2/g for pristine SSMMP. Samples presented distinct morphology as well as sorption capacities. IL and its increased concentration in the samples negatively influenced CO_2 sorption capacity but played an essential role in CO_2/N_2 selectivity. The best results were obtained from CO_2 sorption values for SSMMP-M1 without IL of 2.07 mmol CO_2/g at 1 bar and 4.93 mmol CO_2/g at 30 bar. In addition, a selectivity of 16.94 for the CO_2/N_2 mixture was achieved for SSMMP-5%-Im(nBu)-I sample. SSMMP particles are easy to obtain with low-cost starting materials used in the low energy and CO_2-free emission synthesis process. The sorption/desorption cycles proved the stability for both pristine and IL functionalized samples.

1. Introduction

Climate change resulting from the growing CO_2 concentration is a significant concern. It is imperative to find an effective way to mitigate this gas, allowing the gradual transformation of a global economy based on fossil fuels to a new one based on low-carbon processes. The post-combustion CO_2 capture technology is considered a strong ally for this gradual transformation, given its high potential for application in retrofit processes (Fawzy et al., 2020; Younas et al., 2020). New propositions of materials for CO_2 capture combining low-cost and environmentally friendly products and processes are mandatory for the success of this technology. Aqueous amines, more specifically monoethanolamine- MEA, are the benchmark for CO_2 capture (Sexton and Rochelle, 2011; Gao et al., 2014; Xiao et al., 2018). Alkanolamines aqueous solution present some drawbacks such as high energy consumption, equipment corrosion, oxidative degradation, and high energy required to solution regeneration (Yu et al., 2012; Dinda, 2013; Espinal et al., 2013; Linneen et al., 2013). Solid sorbents appear as an alternative to aqueous amines due to lower energy requirement, ease maintenance, high tunability, and the lack of liquid waste generation (Nicot and Duncan, 2012; Linneen et al., 2013). Many kinds of solid sorbents are described as efficient for CO_2 capture. These include metal-organic frameworks (MOF) (Sabouni et al., 2014; Olajire, 2018; Younas et al., 2020), zeolitic imidasolate frameworks (ZIF) (Zhang et al., 2011; Kinik et al., 2016; Mohamedali et al., 2018), zeolites (Du et al., 2014; Wang et al., 2017; Nikolaidis et al., 2018; Kodasma et al., 2019), activated carbon (Chen et al., 2013; Houshmand et al., 2013), molecular basket sorbent (MBS) (Zhang et al., 2017), amine-modified solid sorbents (Chen et al., 2013; Houshmand et al., 2013; Linneen et al., 2013; Liu and Lin, 2013), aerogel based adsorbent (Kong et al., 2014), silica xerogels containing room temperature ionic liquids (RTIL) (dos Santos et al., 2020), mesoporous silica (He and Seaton, 2006; Kamarudin and Alias, 2013; Wang et al., 2015; Loganathan and Ghoshal, 2017; Duczinski et al., 2018; Polesso et al., 2019; Mohamedali et al., 2020), and carbon nanotubes (Razavi et al., 2011; Chen et al., 2013; Houshmand et al., 2013; Linneen et al., 2013; Liu and Lin, 2013).

* Corresponding author at School of Technology PUCRS Brazil.
E-mail address: einloft@pucrs.br (S. Einloft).

https://doi.org/10.1016/j.clay.2022.106572
Received 31 October 2021; Received in revised form 18 May 2022; Accepted 20 May 2022
Available online 9 June 2022

Table 1
Samples used in this work.

Entry	Sample	Description	Reference
1	Talc Luzenac	natural talc from Luzenac, France	
2	ST-M1	synthetic talc	(Dumas et al., 2013b)– process P1
3	ST-M2	synthetic talc	(Dumas et al., 2013b)- process P3
4	SSMMP-M1	synthetic silico-metallic mineral particles	(Dumas et al., 2013b)- P1 talc precursor
5	SSMMP-M2	synthetic silico-metallic mineral particles	(Dumas et al., 2013b)- P3 talc precursor
6	SSMMP-20%-Im(Me)-NTf_2	SSMMP with 20% of Si bearing Im(Me)-NTf_2	(Dumas et al., 2013a)
7	SSMMP-10%-Im(Me)-NTf_2	SSMMP with 10% of Si bearing Im(Me)-NTf_2	(Dumas et al., 2013a)
8	SSMMP-5%-Im (Me)-NTf_2	SSMMP with 5% of Si bearing Im(Me)-NTf_2	Dumas et al., 2013a
9	SSMMP-5%-Im (nBu)-I	SSMMP with 5% of Si bearing Im(nBu)-I	(Dumas et al., 2013a)
10	SSMMP-5%-Im (nBu)-NTf_2	SSMMP with 5% of Si bearing Im(nBu)-NTf_2	(Dumas et al., 2013a)
11	MCM-41-C	commercial MCM-41	
12	MCM-41	synthetic MCM-41	(Meléndez-Ortiz et al., 2014); Comès et al., 2020
13	MCM-48	synthetic MCM-48	(Meléndez-Ortiz et al., 2014; Comès et al., 2020)

Talc is a layered silicate mineral with the ideal formula of $Mg_3Si_4O_{10}(OH)_2$ extensively used in industrial applications (Dumas et al., 2013b, 2013c). Structurally, talc is composed of neutral layers stacks (forming a lamellar structure) linked together by weak Van Der Waals interactions (Claverie et al., 2018). In these layers, the atoms are linked together by covalent bonds. Its basal faces are not very reactive and constitute 90% of this material surface (Bremmell and Addai-Mensah, 2005; Claverie et al., 2018). The lateral surfaces are considered more reactive, containing SiOH and MgOH (Claverie et al., 2018). Despite its low price and high availability, natural talc presents some disadvantages depending on the intended application, such as a chemical inhomogeneity with the presence of natural cationic substitutions in the structure, mineralogical impurities with the presence of other crystalline phases (carbonates, sulfides, among others), and particle size distribution corresponding mainly to micrometer particles. To specifically answer to applications, it is possible to tailor synthetic talc in terms of composition, crystallinity, particle size, and layer thickness playing on synthesis parameters (Dumas et al., 2013b, 2013c). SSMMP are formed in the first stage of synthetic talcs and can also be named amorphous or short-range nano talcs (Claverie et al., 2018). These materials undergo no hydrothermal process where the lamellar structure formation occurs by stacking octahedral and tetrahedral sheets (TOT). Therefore, the SSMMP particles present an amorphous structure, consisting of some Mg-octahedrons linked with Si-tetrahedrons distributed in the lower and upper part (Dumas, 2013; Dumas et al., 2015; Claverie et al., 2018). Unlike talc, these talc precursor materials have many reactive groups (Si-OH and Mg-OH) free on their surface (Chabrol et al., 2010; Dumas, 2013; Claverie et al., 2018). Among the applications already presented for these materials are the absorption of organic compounds (Ciesielczyk and Krysztafkiewicz, 2007; Ciesielczyk et al., 2007a, 2007b) and polymer fillers (Dietemann, 2012; Dias et al., 2015, 2016; Prado et al., 2020). The synthesis of talc precursors grafted with ionic liquids, using a fast, one-pot method, with low energy expenditure and using only an aqueous medium for dissolving the reagents, was patented (Dumas et al., 2013a). This invention presented new possibilities for applying these materials, such as catalysis and gas selective sorption processes.

Ionic liquids (IL) are appointed as energy-efficient and environmentally benign solvents for CO_2 capture (Nonthanasin et al., 2014) due to their excellent properties. Low vapor pressure and flammability are achieved by different possibilities of combining anions and cations (Muldoon et al., 2007; Hasib-ur-rahman et al., 2010; Nonthanasin et al., 2014). However, high cost and viscosity are the main drawback of these materials (Hasib-ur-rahman et al., 2010).

To be a viable candidate for industrial application, a solid sorbent must be easy to produce on a large scale, at low cost, using environmentally friendly reactants, and easy to regenerate as well. Synthetic talc can also be a candidate for CO_2 capture. Moreover, the possibility of functionalizing it with ionic liquids (Dumas et al., 2013a; Dumas et al., 2014a, 2014b) appears as an excellent opportunity to create highly selective and low-cost materials.

Low cost and energy demand pristine and IL functionalized SSMMP were synthesized and characterized in this work. Synthetic talcs were also obtained through hydrothermal treatment of SSMMP. Samples were evaluated as solid sorbents in CO_2 sorption tests at 25 °C of temperature and pressure up to 30 bar. Yet, sample recyclability and CO_2/N_2 selectivity were also evaluated.

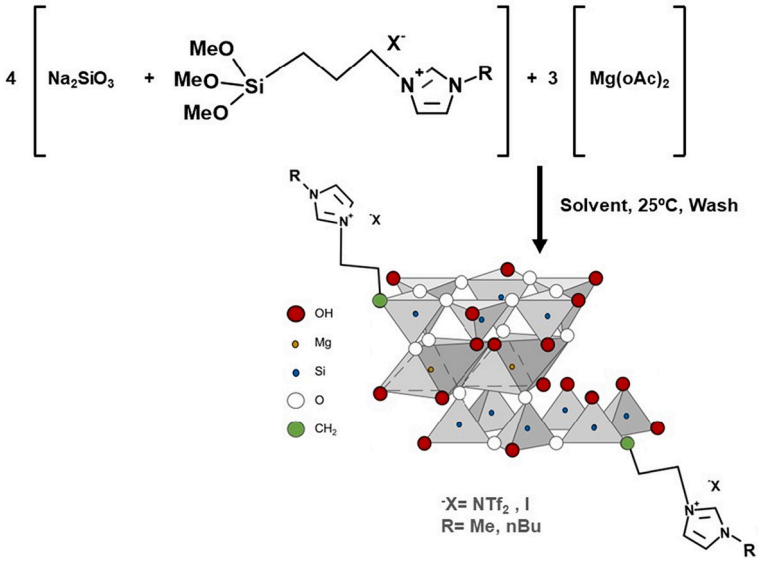

Fig. 1. Scheme of the SSMMP-IL synthesis.

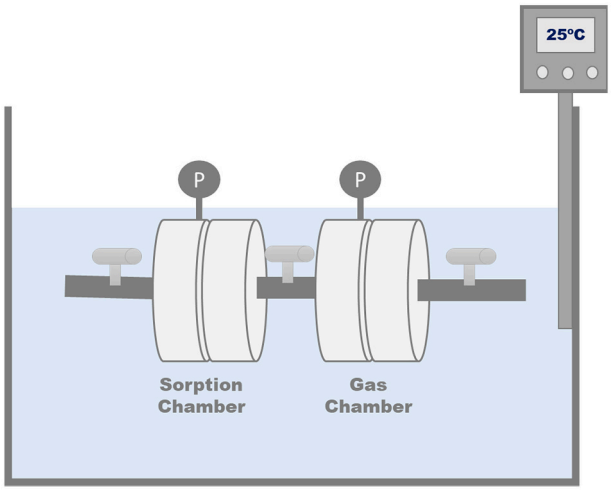

Fig. 2. System for measuring CO_2 sorption capacity.

2. Materials and methods

The synthetic talc (ST) and synthetic silico-metallic mineral particles SSMMP were synthesized using synthetic methods based on the literature, as shown in Table 1. In addition, for comparison purposes, commercial zeolite MCM-41-C (Sigma Aldrich), synthetic zeolites MCM-41 and MCM-48, and natural talc from Luzenac were also tested for CO_2 sorption (Table 1, entries 11–13 and 2 respectively). The natural talc sample comes from a deposit near Luzenac, in the Occitanie region, France. All chemical reagents used in this work were purchased from Sigma Aldrich and used with no further purification.

2.1. ST-M1 and SSMMP-M1 synthesis

Samples were synthesized using magnesium chloride hexahydrate, sodium metasilicate pentahydrate, and hydrochloric acid (1 M solution). ST-M1 (Table 1 entry 2) was synthesized according to the P1 process described in Dumas et al., 2013b, and the hydrothermal reaction was performed at 300 °C for 6 h. SSMMP-M1 (Table 1 entry 4) is a talc precursor synthesized with P1 process described in Dumas et al., 2013b, undergoing no hydrothermal treatment.

2.2. ST-M2, SSMMP-M2 and SSMMP-IL synthesis

For the synthetic talc ST-M2 and SSMMP-M2 preparation (Table 1 entries 3 and 5), the following reagents were used: magnesium acetate tetrahydrate as Mg source, sodium metasilicate pentahydrate as Si source and acetic acid (1 M solution). Dumas et al., 2013b described the P3 process used in their synthesis. The hydrothermal treatment of ST-M2 was carried out at 300 °C for 6 h. SSMMP-M2 is a talc precursor, i.e. it has undergone no hydrothermal treatment. For SSMMP-IL synthesis, corresponding to SSMMP functionalized with imidazolium molecules (Table 1 entries 6–10), the following reagents were additionally used: 1-(triethoxysilylpropyl)-3-methylimidazolium chloride [Im(Me)-Cl-silane], 1-(triethoxysilylpropyl)-3-n-butylimidazolium chloride [Im(nBu)-Cl-silane], sodium iodide and bis(trifluoromethane)sulfonimide lithium salt [$LiNTf_2$]. The synthesis method of SSMMP-IL samples was described in the patent application WO2013093339 (Dumas et al., 2013a), and the synthesis reaction shown in Fig. 1. Samples functionalized with Im(nBu)-NTf_2 and Im(nBu)-I were obtained by replacing 5% of Si source by Im(nBu)-Cl-silane. After a classical exchange of Cl^- by NTf_2 anion (using $LiNTf_2$) and I^- (by using sodium iodide), SSMMP-5%-Im(nBu)-NTf_2 and SSMMP-5%-Im(nBu)-I were further obtained. Samples functionalized with Im(Me)-NTf_2 were synthesized by replacing 5%, 10% and 20% of Si source by Im(Me)-Cl-silane and making a classical exchange of Cl^- by NTf_2 anion (using $LiNTf_2$), resulting in SSMMP-5%-Im(Me)-NTf_2, SSMMP-10%-Im(Me)-NTf_2 and SSMMP-20%-Im(Me)-NTf_2, respectively.

2.3. MCM-41 and MCM-48 synthesis

The synthesis of MCM-41 and MCM-48 (Table 1, entries 12 and 13 respectively) were performed according to the methodology described by Meléndez-Ortiz et al., 2014, and carried out using tetraethoxysilane (TEOS), ammonium hydroxide (29% aqueous solution), and cetyltrimethylammonium bromide (CTAB). The calcination step was based on the method described by (Comès et al., 2020). MCM-41 synthesis was performed by adding 2.5 g of CTAB to 480 ml of deionized water. The solution was stirred and heated to 100 °C. When the solution became translucent, keeping the temperature and stirring constant, 170 ml of ethanol was added. Subsequently, 50 ml of the ammonia solution was added to the mixture, and after another 5 min of stirring, 10 ml of TEOS was added as well and stirred for another 3 h. The sample was washed with deionized water and dried at 100 °C. CTAB was removed from the sample by incineration at 550 °C for 8 h. For the synthesis of MCM-48, 5.2 g of CTAB were added to 240 g of deionized water under constant agitation, then 100 ml of ethanol and 24 ml of the ammonia solution and finally, 6.8 g of TEOS. The solution remained under constant stirring for 16 h at room temperature, then was washed and dried in the oven. CTAB was removed from the sample incineration at 550 °C for 8 h.

3. Material characterization

Thermogravimetric analysis (TGA) were obtained using a TA Instrument SDT-Q600. The temperature range was set at 25 °C–1100 °C with a heating rate of 10 °C/min and under a nitrogen atmosphere. Fourier transform infrared spectroscopy (FT-IR) was performed using Perkin-Elmer FT-IR Spectrum 100 spectrometer in the range of 4000 cm^{-1} to 600 cm^{-1}. RAMAN spectrograms were obtained by a alpha300 R access confocal Raman microscopy system from WiTec GmbH, equipped with a UHTS 300 spectrophotometer with a diffraction grating of 600 g/mm BLZ = 500 nm and using a He-Ne laser. The nitrogen adsorption-desorption isotherms were determined at 77 K, using a volumetric method with a Quantachrome Autosorb-1 apparatus. The isotherms were recorded in the 0.05–0.3 relative pressure range, using high purity nitrogen. Samples were outgassed for 15 h at 120 °C under vacuum before analysis. Specific surface areas were calculated using the Brunauer-Emmett-Teller (BET) method (Brunauer et al., 1938). X-ray diffraction (XRD) analyses were performed on disoriented powders, using a Bruker D8 Advance diffractometer operating under the reflection of the $CuK\alpha_{1+2}$ radiation (λ = 1.5418 Å), $K\alpha_2$ being substracted with Bruker Diffrac.Eva software for figures. XRD patterns were collected at room temperature over the 2–80°2θ range, using 0.4 s counting time per 0.01°2θ step. Solid-state ^{29}Si CP/MAS NMR spectrum was recorded on a 400 MHz Bruker Avance III spectrometer (LCC laboratory, Toulouse, France) in a static field of 9.4 T at resonance frequency of 79.49 MHz. Measurement was performed on powder in ZrO_2 rotors of 4.0 mm at a spinning frequency of 10 kHz and a 3 ms CP pulse. Chemical shift is relative to tetramethylsilane (TMS). The powdered talcs skeletal density (ρs) was measured at 25 °C using an Ultrapycnometer 1000 - Quantachrome Corporation pycnometer using ultra-high purity helium (Air Liquide / 99.999%). The particles morphology was assessed using a field emission scanning electron microscope (FESEM), Inspect F50 equipment (FEI Instruments).

3.1. CO_2 adsorption measurements

CO_2 sorption capacity was measured in an equilibrium cell (Fig. 2) equipped with two chambers (one being a gas chamber and the other a sorption chamber), using the pressure decay technique reported by KOROS and PAUL (Koros and Paul, 1976).

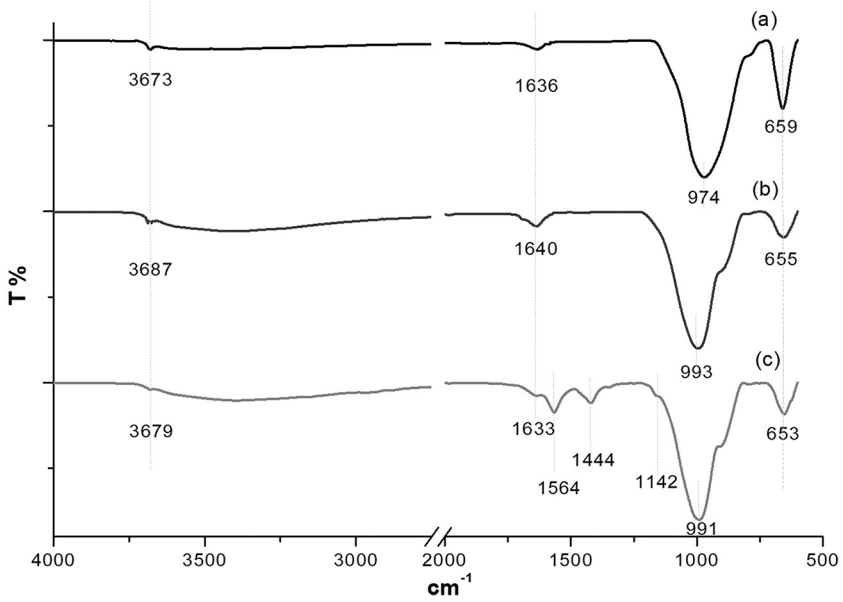

Fig. 3. FTIR spectra of (a) ST-M2, (b) SSMMP-M2 and (c) SSMMP-5%-Im(nBu)-I.

Table 2
Thermogravimetric analyses results.

Entry	Sample	1 st mass loss		2 nd mass loss		3 rd mass loss	
		T (°C)	*w/w %*	*T (°C)*	*w/w %*	*T (°C)*	*w/w %*
1	Talc Luzenac	–	–	–	–	774–1084	4.6
2	ST-M1	20–150	10.8	150–830	5.5	–	–
3	ST-M2	26–152	0.3	152–598	4.4	598–865	3.5
4	SSMMP-M1	24.3–281.8	20.3	281.8–791.7	6.9	–	–
5	SSMMP-M2	25.8–159.9	10.5	159.9–417.2	6.9	417.2–850.9	4.5
6	SSMMP-20%-Im(Me)-NTf_2	29–234	11.8	234–708	28.4	–	–
7	SSMMP-10%-Im(Me)-NTf_2	29–232	19.9	232–782	20.9	–	–
8	SSMMP-5%-Im(Me)-NTf_2	38–170	18.8	170–584	18.4	–	–
9	SSMMP-5%-Im(nBu)-I	26–250	18.8	250–643	12.6	–	–
10	SSMMP-5%-Im(nBu)-NTf_2	22–286	18.7	286–712	11.7	–	–
11	MCM-41-C	44.6–795	2.6	–	–	–	–
12	MCM-41	46–791.3	19.6	–	–	–	–
13	MCM-48	22.8–791.7	26.4	–	–	–	–

The materials' CO_2 sorption capacity was performed according to the methodology described in previous works (Bernard et al., 2017, 2018; Rojas et al., 2017; dos Santos et al., 2020). The tests were carried out in triplicates, at a constant temperature of 25 °C, and CO_2 (Air Liquide, 99.998%) pressure varying from 0 to 30 bar. Before each test, samples were dried in an oven at 100 °C for five hours. The sample mass used in the tests ranged from 0.6 g to 0.9 g. Before each new analysis, the sample was placed in an oven, where it remained for 1 h at 110 °C for CO_2 desorption. Samples with the best CO_2 sorption capacity and CO_2/N_2 selectivity were submitted to sorption/desorption tests 10 times. To corroborate sample stability after 10 cycles, BET and FTIR analysis were performed.

3.2. CO_2/N_2 selectivity evaluation

Material selectivity was determined according to the procedure described in the literature by Azimi and Mirzaei, 2016. The same CO_2 sorption system described above was used for the selectivity tests, replacing the pure CO_2 gas with a standard gas mixture with a composition of 15:85 (*v*/v) of CO_2/N_2. Selectivity tests were carried out at an equilibrium pressure of 20 bar at 25 °C. The gas composition of the mixture at the exit of the system was measured using a gas chromatograph (GC) (Shimadzu GC-14B) equipped with a thermal conductivity detector. The samples selectivity was determined by Eq. (1), where X_{CO2} and X_{N2} correspond to the molar fractions of CO_2 and N_2 sorbed by the sample, and Y_{CO2} and Y_{N2} are the molar fractions of CO_2 and N_2 present in the gas phase, respectively (Azimi and Mirzaei, 2016; Duczinski et al., 2018; Polesso et al., 2019).

$$S = \frac{X_{CO_2}/Y_{CO_2}}{X_{N_2}/Y_{N_2}} \quad (1)$$

4. Results

Fig. 3 shows the infrared spectroscopy analysis of characteristic samples of synthetic talc, SSMMP, and SSMMP functionalized with IL (ST-M2, SSMMP-M2, and SSMMP-5%-Im(nBu)-I, respectively). The characteristic bands near 3700 cm^{-1} and 655 cm^{-1}, appearing in all samples, are attributed to Mg_3-OH bond (Schroeder, 2002; Dias et al., 2015). The wide band between 3650 and 3000 cm^{-1} is related to the -OH of the water molecules corroborated by the band near 1635 cm^{-1} (Mor et al., 2017; Duczinski et al., 2018; Ouyang et al., 2018). The characteristic bands of Si-O and Si-O-Si bonds appear between 1050 and 900 cm^{-1} (Dias et al., 2015; Ouyang et al., 2018).

Fig. 3 (c), samples containing IL, shows the appearance of three new characteristic bands. The band formed in the region of 1564 cm^{-1} is

Table 3
Sample physical parameters.

Entry	Sample	Specific surface area (m^2/g)	Density (g/cm^3)
1	Talc Luzenac	20	2.70
2	ST-M1	329	2.53
3	ST-M2	125	2.71
4	SSMMP-M1	354	2.55
5	SSMMP-M2	325	2.31
6	SSMMP-20%-Im(Me)-NTf_2	5	2.21
7	SSMMP-10%-Im(Me)-NTf_2	55	1.90
8	SSMMP-5%-Im(Me)-NTf_2	79	1.96
9	SSMMP-5%-Im(nBu)-I	156	2.05
10	SSMMP-5%-Im(nBu)-NTf_2	151	2.23
11	MCM-41-C	841	2.33
12	MCM-41	1188	2.42
13	MCM-48	1361	1.89

Table 4
CO_2 sorption values for all samples at 1, 10 and 30 bar.

Entry	Sample	mmol CO_2/g sorbent at 1 bar	mmol CO_2/g sorbent at 10 bar	mmol CO_2/g sorbent at 30 bar
1	Talc Luzenac	0.50	0.68	0.79
2	ST-M1	0.08	0.15	0.35
3	ST-M2	0.19	0.38	0.74
4	SSMMP-M1	2.07	3.19	4.93
5	SSMMP-M2	1.86	3.78	6.32
6	SSMMP-20%-Im(Me)-NTf_2	0.37	0.63	0.56
7	SSMMP-10%-Im(Me)-NTf_2	0.50	1.05	1.00
8	SSMMP-5%-Im(Me)-NTf_2	0.58	1.47	1.68
9	SSMMP-5%-Im(nBu)-I	0.89	1.54	2.16
10	SSMMP-5%-Im(nBu)-NTf_2	0.95	1.69	2.02
11	MCM-41-C	0.40	2.04	5.25
12	MCM-41	1.58	4.12	6.21
13	MCM-48	1.71	4.28	7.75

attributed to the C═C bond of the imidazolium ring, the band around 1444 cm^{-1} related to the deformation of the CH_2 group of the IL (Duczinski et al., 2018) and the shoulder formed in the region 1142 cm^{-1} related to the Si-C bond present in the imidazolium lateral chain (Maria and Airoldi, 2001).

Raman spectroscopy analysis was performed for SSMMP-M2, SSMMP-5%-Im(nBu)-I and SSMMP-5%-Im(nBu)-NTf2 samples. A band in the region of 680 cm^{-1}, appearing in the Raman spectra of all samples, is attributed to the Si-O-Si symmetrical elongation mode, present in the SSMMP structure (see Fig. S1) (Kloprogge, 2017). In the spectra of samples containing IL, the appearance of weak bands near 1400 cm^{-1} is attributed to the in plane asymmetric stretch of the imidazole ring (H-C-H, C-C and C-N bonds) (Talaty et al., 2004; Chen et al., 2017; Paschoal et al., 2017). The bands in the region from 2839 to 3066 cm^{-1} are attributed to the cation lateral chains and imidazolium ring C-H bonds stretching (Grondin et al., 2011; Chen et al., 2017).

Synthesized samples were characterized by thermogravimetric analysis (see Table 2). Results show that all samples, except the natural talc sample (Table 2, entry 1), have a first mass loss starting between 20 °C–46 °C. This first mass loss is attributed to the loss of physisorbed water (Dumas et al., 2013c; Duczinski et al., 2018). For MCM-41-C, MCM-41, and MCM-48 (Table 2, entries 11–13 respectively), only this first mass loss at low temperatures was observed, indicating that all the surfactant used in the MCM-41 and MCM-48 synthesis was removed in the calcination step. The second mass loss refers to the loss of silanols (Si-OH) and magnesium hydroxide (Mg-OH) present on the synthetic talc sheet edges (Table 2, entries 2 and 3) (Dumas et al., 2013c) and in the SSMMP surface (Table 2, entries 4–10). For samples grafted with IL, this second mass loss is also related to the loss of the imidazolium cation (Dumas et al., 2013c; Seyed and Nazemzadeh, 2017; Duczinski et al., 2018). Thus, particle size allied to the presence of the imidazolium cation are responsible for the significant variation on the second mass loss. Natural talc (Table 2, entry 1) showed higher thermal stability, evidencing no mass loss at low temperatures due to its hydrophobicity. A single-step mass loss was observed at high temperature (774 °C to 1084 °C), corresponding to the talc sheets dehydroxylation, ocurring simultaneously with the enstatite crystallization and the silica formation (Chabrol et al., 2010). For ST-M1 and ST-M2 synthetic talcs, and their precursors SSMMP-M1 and SSMMP-M2 (Table 2, entries 2, 3, 4 and 5, respectively), dehydroxylation, enstatite crystallization and silica formation steps occurred in different ways. For ST-M1 and SSMMP-M1 samples, this step occurs continuously (corresponding to the second mass loss), and for ST-M2 and SSMMP-M2 in two distinct steps corresponding to the second and third mass loss, here attributed to the dehydroxylation of the sheet edges and of the bulk, respectively (Chabrol et al., 2010; Dumas et al., 2013c). Typical thermograms are presented in the supplementary file (Figs. S2-S4).

BET measurement was also used to characterize the samples. As seen in Table 3, the synthetic talcs ST-M1 and ST-M2 (329 m^2/g and 125 m^2/g, respectively) present higher specific surface area values when compared to natural talc from Luzenac (20 m^2/g). For SSMMP-IL, functionalized with imidazolium molecules, increasing imidazolium content decreases the specific surface area values (compare SSMMP-5%-Im(Me)-NTf_2, 79 m^2/g; SSMMP-10%-Im(Me)-NTf_2, 55 m^2/g; and SSMMP-20%-Im(Me)-NTf_2, 5 m^2/g). Silica gel immobilized with tetraethylenepentamine (Nonthanasin et al., 2014) shows the same behavior as SSMMP-IL samples. In addition, the decrease in the samples' specific surface area with increasing ionic liquid concentration indicate that the functionalization of SSMMP-M1 with imidazolium molecules was successful (Younas et al., 2020). The synthetic method directly influences the specific surface area values (compare samples ST-M1, 329 m^2/g and ST-M2, 125 m^2/g). Table 3 also shows the density values of the samples under study in the range of 1.89–2.70 g/cm^3, attributed to the similarity of the structure of synthetic samples with the one of natural talc, and the presence of functional groups attached to their structure for the functionalized samples.

XRD analysis (Fig. S5) shows for ST-M1 and ST-M2 the presence of intense diffraction peaks, very similar to those found for Luzenac talc corroborating the crystallinity of these materials (Dias et al., 2015; Prado et al., 2020). SSMMP-5%-Im(Bu)-I present an X-ray diffraction pattern with broad and low-intensity diffraction peaks, confirming the lower stacking order and growth in the ab plane, and the amorphous structure (Claverie et al., 2018).

NMR analysis confirms that organic groups are well present in the precursor structure. ^{29}Si NMR spectra (Fig. S6) shows two signals regions. The first one between −75 and − 95 ppm corresponds to Q-type Si atoms (with Si-O-Si, Si-O-Mg and Si-OH bonds), probably Q^1 and Q^2 for the most part because of the small TOT entities of the precursor (based on literature, please see discussion in the next paragraph). The second region between −40 and − 65 ppm corresponds to T-type Si atoms with Si-C bond, more probably T^1 around −49 ppm and T^2 around −53 ppm (basing upon reported studies, for example Fuji and Hayashi, 2005, or Gallégo et al., 2008). These results indicate that the organic group is covalently bonded with the phyllosilicate-like structure of SSMMP (see structure in Fig. 1).

Table 4 and Fig. 4 present the CO_2 sorption capacity test results for each of the synthesized samples, at equilibrium pressures of 1–30 bar of CO_2 at a temperature of 25 °C. When comparing the results of CO_2 sorption capacity of ST-M1 and ST-M2 (Table 4, entries 2 and 3,

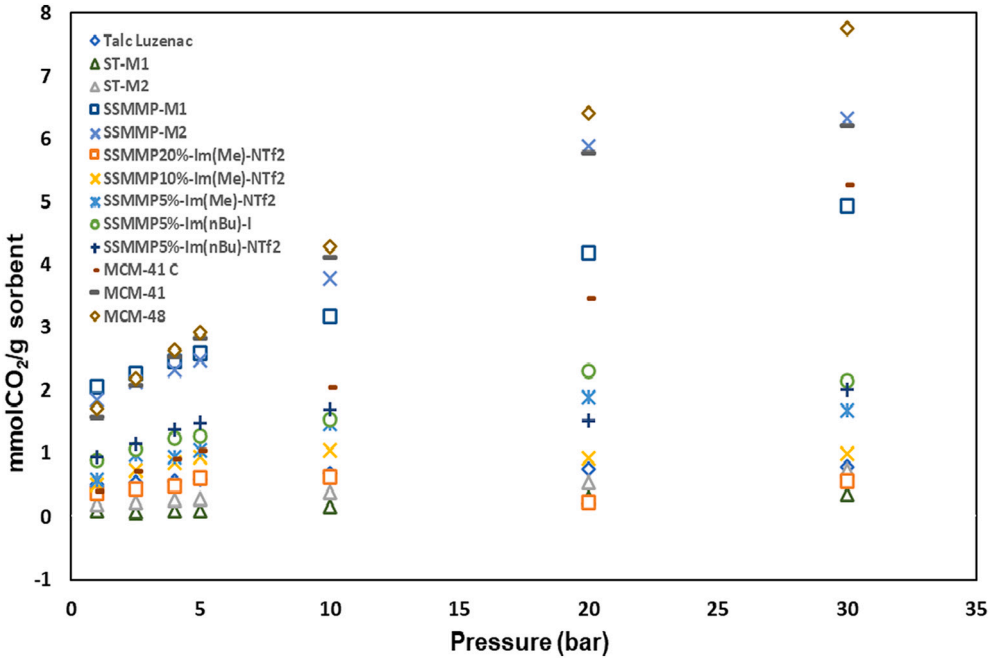

Fig. 4. Behavior of the samples as sorbents for CO_2 capture at 25 °C and a pressure range of 1–30 bar.

Table 5
CO_2 sorption values for different inorganic silicate materials found in the literature.

Sample	Sample type	mmol CO_2/g sorbent	Analysis conditions	Reference
SX	Silica xerogel	1.13	1 bar; 25 °C	(dos Santos et al., 2020)
MCM-41-30	Mesoporous silica	<0.5	1 bar; 30 °C	(Loganathan and Ghoshal, 2017)
SBA-15	Mesoporous silica	0.45	1 bar; 45 °C	(Sanz et al., 2010)
MCSU-H	Mesoporous silica	<0.2	1 bar; 40 °C	(Fujiki et al., 2015)
$NaMnSi_{10}O_x$	Metal silicate	<1.8	1 bar; 25 °C	(Li et al., 2020)
$NaNiSi_{10}O_x$	Metal silicate	<0.9	1 bar; 25 °C	(Li et al., 2020)
$NaCuSi_{10}O_x$	Metal silicate	<1.6	1 bar; 25 °C	(Li et al., 2020)
MMT	Porous Montmorillonite	<0.5	1 bar; 25 °C	(Atilhan et al., 2016)
E-VER	Exfoliated Vermiculite	<1.0	1 bar;25 °C	(Zhang et al., 2020)
SSMMP-M1	Talc precursor	2.07	1 bar; 25 °C	This work

respectively) with their respective precursors (precipitated material without hydrothermal process) SSMMP-M1 and SSMMP-M2 (Table 4, entries 4 and 5), we observed that for both precursor materials, CO_2 sorption capacity was higher than for ST at all CO_2 equilibrium pressures. At equilibrium pressure of 1 bar, SSMMP-M1 evidenced a CO_2 sorption capacity of 2.07 mmol CO_2/g, an increase of 1.99 mmol CO_2/g, compared to ST-M1 (0.08 mmol CO_2/g, 1 bar CO_2). This higher sorption capacity of SSMMP is directly related to the distinct structures presented by the precipitated materials (SSMMP-M1 and SSMMP-M2) compared to synthetic talcs obtained after hydrothermal treatment process. Literature (Chabrol et al., 2010; Dumas et al., 2015; Claverie et al., 2018) points out that unlike ST, presenting a lamellar shape with several stacked layers, the precipitated SSMMP, before going through hydrothermal treatment process, consists of structures composed of small TOT entities, formed by Mg-octahedrons [$MgO_4(OH)_2$] and Si-tetrahedrons (SiO_4) distributed in the lower and upper part of its Mg-octahedral "sheet" resulting in a structure with a number of Si-OH and Mg-OH reactive groups on their surfaces. When the precipitated material (SSMMP) is subjected to hydrothermal treatment, both the Mg-octahedral sheet and the two Si-tetrahedron sheets grow in the (ab) crystallographic plane and along the c axis, with a large amount of Si-tetrahedrons connected to three other Si-tetrahedrons and only few ones connected to only two or one Si-tetrahedrons (located on the edge of the sheets). The same happens for the Mg-octahedral sheet (Chabrol et al., 2010; Dumas et al., 2013c, 2015; Claverie et al., 2018). According to literature (Bremmell and Addai-Mensah, 2005), only 10% of talc surfaces have Si-OH and Mg-OH reactive groups, present only in small amounts on the talc side surface (Claverie et al., 2018). These groups (-SiOH and -MgOH) present high affinity to CO_2, so the greater amount of these groups on the SSMMP surface is responsible for the higher CO_2 sorption capacity of these samples when compared to their respective synthetic talc (Rimola et al., 2013; Polesso et al., 2019). For SSMMP-IL, as seen in Table 4, the increase in the IL content caused a decrease in CO_2 sorption capacity, lower for all SSMMP-IL than for SSMMP-M1 and SSMMP-M2 regardless of the analyzed equilibrium pressures. SSMMP-M2 exhibited CO_2 sorption capacity of 95,8% (1 bar), 123,7% (10 bar) and 212,9% (30 bar) higher than SSMMP-5%-Im(nBu)-NTf_2. The CO_2 adsorption process on the IL and the SSMMP surface is physical; there is no chemical reaction between the material and the CO_2 (Ramdin et al., 2012; Houshmand et al., 2013). The incorporation of imidazolium molecules in the sample results in a decrease in the specific surface area of SSMMP-M2, decreasing its CO_2 sorption capacity due to limited interactions of SSMMP/CO_2 (Ramdin et al., 2012). These results evidenced the relevance of the SSMMP/CO_2 interaction compared to the IL/CO_2. As previously discussed, SSMMP-M1 and M2 have an amorphous structure consisting of small TOT entities (Dumas et al., 2015), containing several reactive groups (-SiOH and -MgOH) on their surface which can interact with CO_2. Increasing in the IL load results in a decrease in both the SSMMP specific suface area and surface reactive groups, consequently reducing SSMMP/CO_2 interaction (Ramdin et al., 2012; Rimola et al., 2013; Kinik et al., 2016; Polesso et al., 2019). Malherbe et al. (2010) analyzed the CO_2 molecule interaction with different silica-based materials surface. They stated that the interaction between CO_2/silica surface occurs by physical adsorption through dispersive and electrostatic interactions and by CO_2 weak interaction with the OH group present in the silica surface ($H^{\delta+} \cdots {}^{\delta-}O{=}C{=}O^{\delta-}$).

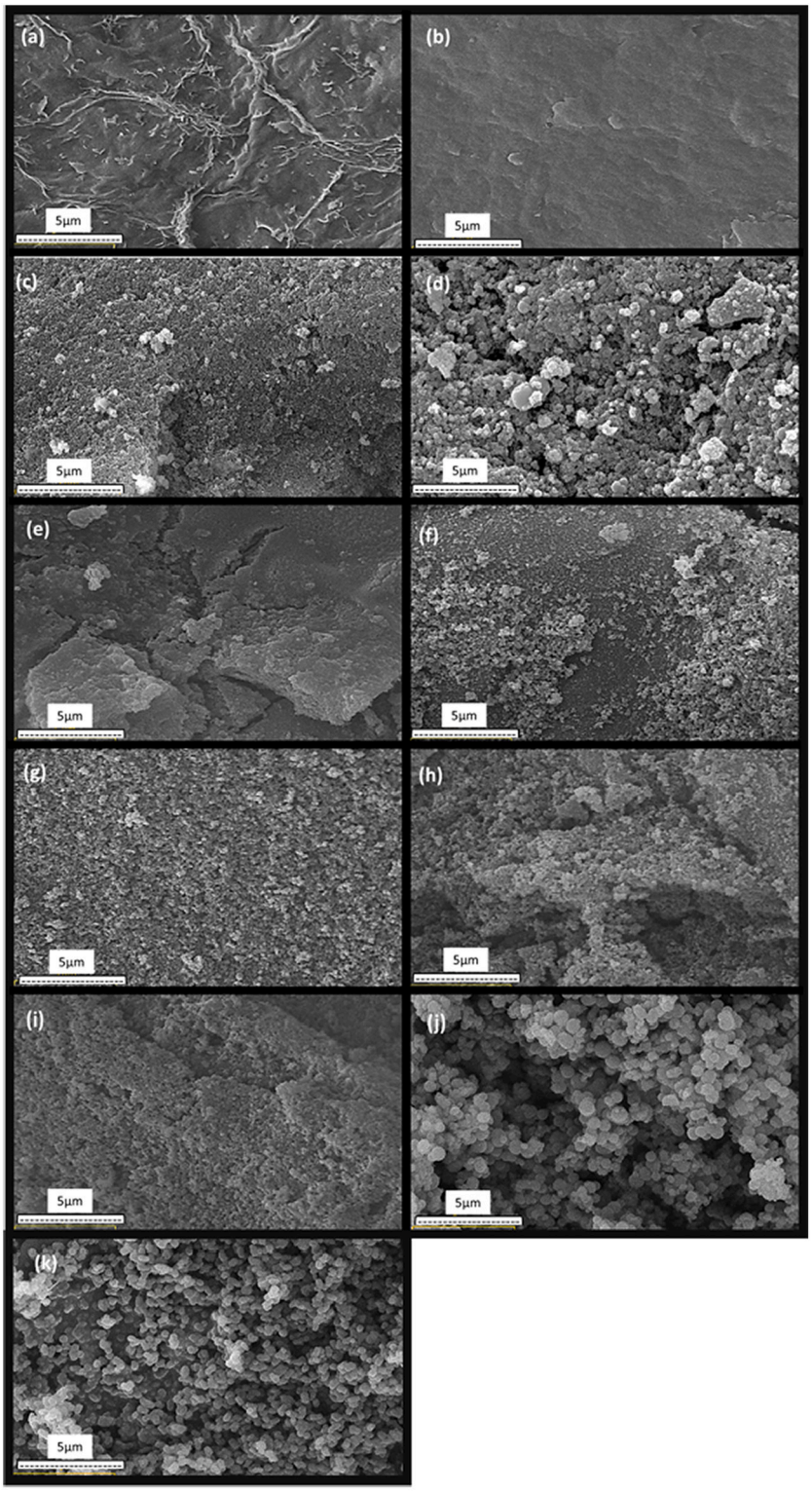

Fig. 5. SEM images of (a) ST-M1, (b) ST-M2, (c) SSMMP-M1, (d) SSMMP-M2 (e) SSMMP-20%-Im(Me)-NTf_2, (f) SSMMP-10%-Im(Me)-NTf_2, (g) SSMMP-5%-Im(Me)-NTf_2, (h) SSMMP-5%-Im(nBu)-I, (i) SSMMP-5%-Im(nBu)-NTf_2, (j) MCM-41 and (k) MCM-48.

Our group demonstrated that for IL grafted in silica-based solids, the anion size and charge density play an important role in CO_2 sorption capacity being the solid biding sites the primary driver for CO_2 capture (Aquino et al., 2015). It was also evidenced that CO_2 establish weaker interactions with the cation showing no competition with the anion for the same locations. The preferred location for the CO_2 molecule in the IL is near methyl groups explained by the existence of a local conformational equilibrium and, consequently, a higher cavity formation probability (Corvo et al., 2013). These finds, combined with the results presented by Simon et al. (2018), evidencing that the increase in the cation carbon chain increases the CO_2 sorption capacity in the IL, corroborate the results of this work evidencing the higher sorption capacity achieved by the SSMMP grafted with the IL containing the Im $(nBu)^+$ cation (entries 9 and 10, Table 4) compared to $Im(Me)^+$ (entries

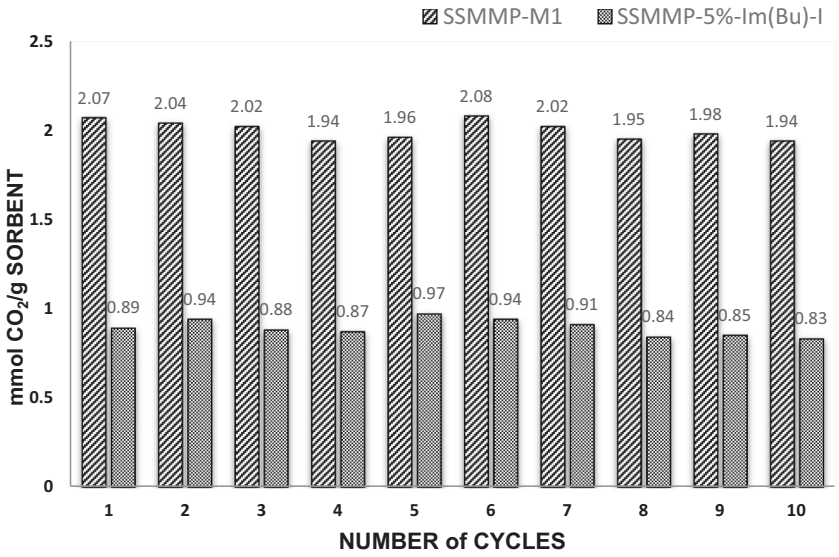

Fig. 6. CO_2 sorption/desorption test for SSMMP-M1 and SSMMP-5%-Im(nBu)-I at 1 bar and 25 °C.

6 to 8, Table 4).

These results indicate that an ideal balance between the IL and OH content allied to specific surface area value would be necessary to achieve an adequate CO_2 absorption capacity.

Comparing SSMMP-M1 and SSMMP-M2, one can see that the sample specific surface area only influenced CO_2 sorption capacity at low pressures (up to 5 bar). SSMMP-M1 exhibited a surface area 8.9% superior to SSMMP-M2 and sorption capacity 9.5% higher than SSMMP-M2 at 1 bar of CO_2 equilibrium pressure. For all pressures above 10 bar, the SSMMP-M1 presented the best sorption capacity performance.

Mesoporous silica MCM-41-C, MCM-41, and MCM-48 were also evaluated for CO_2 sorption as well-known solid sorbents and support materials for capturing CO_2 (He and Seaton, 2006; Kamarudin and Alias, 2013; Wang et al., 2015; Loganathan and Ghoshal, 2017; Mohamedali et al., 2020). Comparing these three materials with SSMMP-M1 and SSMMP-M2, it is observed (Fig. 4) that, up to 2.5 bar, these last showed higher sorption capacity than the mesoporous silica and up to 20 bar compared to MCM-41-C. At higher pressures from 4 bar, MCM-41 and MCM-48 have greater sorption capacity compared to SSMMP-M1 and SSMMP-M2, except for MCM-41 similar but just below SSMMP-M2 above 20 bar. However, as the primary purpose of these materials is to capture CO_2 in post-combustion processes, where the CO_2 partial pressure is 1 bar, SSMMP-M1 and, to a lesser extent, SSMMP-M2 are still considered the best materials. Furthermore, they are synthesized in just one step (one-pot), quantitative precipitation showing excellent atom economy process, with low-cost reagents and no energy expenditure (no hydrothermal treatment or calcination step).

Table 5 presents sorption capacity (at 1 bar) of other inorganic silicate materials described in literature. It is clear from this table that SSMMP-M1 presents greater CO_2 sorption capacity at low pressure. Moreover, SSMMP-M1 is cheaper when compared with other solid sorbents considered suitable for capturing CO_2 at low pressure, such as MOFs (Mg-MOF-78 in (Yu and Balbuena, 2013) and ZIFs (IL@ZIF-8 in (Mohamedali et al., 2018). Furthermore, MOFs are considered expensive materials to produce, unstable in basic and acidic solutions and humid environments, turning their commercial application highly limited (Yu and Balbuena, 2013; Younas et al., 2020). On the other hand, ZIFs, (a subfamily of MOFs) present a greater or comparable sorption capacity with SSMMP-M1 only when impregnated with ILs (Mohamedali et al., 2018).

Fig. 5 highlights that morphology appears to play a role in CO_2 capture. It is possible to observe that samples ST-M1 and ST-M2 (entries (a) and (b)) have a compact and ordered surface compared to all other studied samples (SSMMP-M1, SSMMP-M2, all SSMMP-IL samples, MCM-41 and MCM-48). The two latter have relatively smaller particles and rougher surface. ST-M1, Talc Luzenac, ST-M2, and SSMMP-20%-Im (Me)-NTf_2 have low CO_2 sorption capacity, less than 1 mmol CO_2/g of sorbent even at 30 bar of CO_2 pressure. All other samples have sorption capacity equal to or greater than 1 mmol CO_2/g- of sorbent at 30 bar.

Fig. 5 highlights that morphology appears to play a role in CO_2 capture. It is possible to observe that samples ST-M1 and ST-M2 (entries (a) and (b)) have a compact and ordered surface compared to all other studied samples (SSMMP-M1, SSMMP-M2, all SSMMP-IL samples, MCM-41 and MCM-48). The two latter have relatively smaller particles and rougher surface. ST-M1, Talc Luzenac, ST-M2, and SSMMP-20%-Im (Me)-NTf_2 have low CO_2 sorption capacity, less than 1 mmol CO_2/g of sorbent even at 30 bar of CO_2 pressure. All other samples have sorption capacity equal to or greater than 1 mmol CO_2/g- of sorbent at 30 bar.

4.1. *SSMMP-M1 recycle test*

Fig. 6 presents the CO_2 sorption/desorption test results for SSMMP-M1 and SSMMP-5%-Im(Bu)-I. As seen for SSMMP-M1, sorption capacity ranged from 1.94 to 2.08 mmol of CO_2/g during the 10 cycles at 25 °C, presenting an average sorption capacity of 2.00 mmol of CO_2/g. For SSMMP-5%-Im(nBu)-I the sorption capacity variation during the 10 sorption/desorption cycles was 0.83 to 0.97 mmol CO_2/g and its average sorption capacity 0.89 mmol CO_2/g.

To confirm SSMMP-M1 and SSMMP-5%-Im(nBu)-I stability, BET and FTIR analyzes were performed after 10 sorption/desorption cycles. According to the results (Figs. S7 and S8), no structural and surface area changes were observed after recycling.

4.2. *CO_2/N_2 selectivity*

CO_2/N_2 selectivity was evaluated for SSMMP-M1 and SSMMP-5%-Im (nBu)-I. Results indicated that the presence of ILs in the sample increased 124.67% the CO_2 removal (selectivity of 16.94 ± 0.87) compared to pristine SSMMP-M1 (selectivity of 7.54 ± 0.64). The greater CO_2 affinity presented by the sample functionalized with IL is in agreement with other published studies (Harvey et al., 2016; Duczinski et al., 2018; Mohamedali et al., 2018; Polesso et al., 2019). These results indicate that the presence of the IL on the SSMMP surface increased the sample affinity to CO_2 (Nkinahamira et al., 2017; Zhu et al., 2018;

Polesso et al., 2019). The obtained selectivity results proved to be promising when compared to other materials reported in the literature. Mohamedali et al., 2018 analyzed the selectivity of pure ZIF-8 and incorporated with different concentrations of acetate-based ILs samples in CO_2/N_2 mixtures at a pressure of 1 bar and a temperature of 30 °C. For pure ZIF-8, CO_2/N_2 selectivity was 5. For all samples with different concentrations of incorporated IL, the selectivity was 10, corroborating the important effect of ILs in CO_2/N_2 selectivity.

5. Conclusion

This work reported the synthesis, characterization, CO_2 sorption capacity, and CO_2/N_2 selectivity of different synthetic materials. For SSMMP-IL, the decrease in the specific surface area resulting from the increase in the IL content decreased CO_2 sorption capacity due to reducing reactive groups present on the SSMMP surface. Pristine SSMMP-M1 presented an excellent sorption capacity at low pressures (2.07 mmol CO_2/g sorbent at 1 bar) compared to synthetic talc and other solid sorbents presented in the literature. Unlike CO_2 sorption tests, CO_2/N_2 selectivity was improved in the presence of the IL showing an increase of 124% in CO_2 selectivity (CO_2/N_2 mixture) compared to pristine SSMMP-M1. SSMMP-M1 and SSMMP-5%-Im(nBu)-I stabiity was also verified after 10 consecutive CO_2 sorption/desorption cycles. SSMMP-M1 CO_2 sorption capacity and the selectivity of SSMMP-5%-Im (nBu)-I are promising for industrial use in post-combustion capture and separation processes due to the ease of synthesis (one-pot), low cost of reagents, and low energy consumption. There are no heating steps for synthesis or the need for calcination as well, unlike most solid sorbents presented in the literature as suitable materials for capturing CO_2 at low pressures. Concerning material disposal, after many cycles of SSMMP used for CO_2 capture, it can still be used in other applications (hydrothermal process, polymer filler, among others).

CRediT authorship contribution statement

Daniela Rodrigues: Conceptualization, Methodology, Writing, Investigation. **Franciele Bernard**: Conceptualization, Writing, Investigation, Methodology. **Christophe Le Roux**: Conceptualization, Writing, Investigation, Methodology. **Evandro Duarte**: Investigation, Methodology. **Pierre Micoud**: Conceptualization, Writing, Methodology, Investigation. **Alain Castillo**: Conceptualization, Methodology. **François Martin**: Conceptualization, Investigation, Project administration, Funding acquisition. **Sandra Einloft**: Conceptualization, Writing, Methodology, Project administration, Funding acquisition.

Declaration of Competing Interest

None.

Acknowledgment

This study was written by some members of the Capes- PRINT Internationalization Project from PUCRS University and was financed in part by the Coordination for the Improvement of Higher Education Personnel- Brasil (CAPES) – Finance Code 001. Sandra Einloft thanks CNPq for the research scholarship.

Appendix A. Supplementary data

Supplementary data to this article can be found online at https://doi.org/10.1016/j.clay.2022.106572.

References

Aquino, A., Bernard, F., Ligabue, R., Seferin, M., Chaban, V.V., Cabrita, E.J., Einloft, S., 2015. Rationalizing the role of the anion in CO2 capture and conversion using imidazolium-based ionic liquid modified mesoporous silica. Royal Soc. Chem. 5, 64220–64227. https://doi.org/10.1039/c5ra07561k.

Atilhan, M., Atilhan, S., Ullah, R., Anaya, B., Cagin, T., Yavuz, C.T., Aparicio, S., 2016. High-Pressure Methane, Carbon Dioxide, and Nitrogen Adsorption on Amine-Impregnated Porous Montmorillonite Nanoclays, 61, pp. 2749–2760. https://doi.org/10.1021/acs.jced.6b00134.

Azimi, A., Mirzaei, M., 2016. Experimental evaluation and thermodynamic modeling of hydrate selectivity in separation of CO2 and CH4. Chem. Eng. Res. Des. 111, 262–268. https://doi.org/10.1016/j.cherd.2016.05.005.

Bernard, F.L., Polesso, B.B., Cobalchini, F.W., Chaban, V.V., Nascimento, J.F., Vecchia, F. D., Einloft, S., 2017. Hybrid Alkoxysilane-Functionalized Urethane-Imide-based Poly (ionic liquids) as a New Platform for Carbon Dioxide Capture. Energy Fuel 31, 9840–9849. https://doi.org/10.1021/acs.energyfuels.7b02027.

Bernard, F.L., Duczinski, R.B., Rojas, M.F., Fialho, M.C.C., Carreño, L.Á., Chaban, V.V., Vecchia, F.D., Einloft, S., 2018. Cellulose based poly(ionic liquids): Tuning cation-anion interaction to improve carbon dioxide sorption. Fuel 211, 76–86. https://doi.org/10.1016/j.fuel.2017.09.057.

Bremmell, K.E., Addai-Mensah, J., 2005. Interfacial-chemistry mediated behavior of colloidal talc dispersions. J. Colloid Interface Sci. 283, 385–391. https://doi.org/10.1016/j.jcis.2004.09.048.

Brunauer, S., Emmett, P.H., Teller, E., 1938. Adsorption of gases in Multimolecular Layers. J. Am. Chem. Soc. 60, 309–319.

Chabrol, K., Gressier, M., Pebere, N., Menu, M.J., Martin, F., Bonino, J.P., Marichal, C., Brendle, J., 2010. Functionalization of synthetic talc-like phyllosilicates by alkoxyorganosilane grafting. J. Mater. Chem. 20, 9695–9706. https://doi.org/10.1039/c0jm01276a.

Chen, Z., Deng, S., Wei, H., Wang, B., Huang, J., Yu, G., 2013. Activated carbons and amine-modified materials for carbon dioxide capture – A review. Front. Environ. Sci. Eng. 7, 326–340. https://doi.org/10.1007/s11783-013-0510-7.

Chen, F., You, T., Yuan, Y., Pei, C., Ren, X., Huang, Y., Yu, Z., Li, X., Zheng, H., Pan, Y., Yang, K., Wang, L., Chen, F., You, T., Yuan, Y., Pei, C., Ren, X., Huang, Y., 2017. Pressure-induced structural transitions of a room temperature ionic liquid — 1-ethyl-3-methylimidazolium chloride Pressure-induced structural transitions of a room temperature HPSTAR ionic liquid — 1-ethyl-3-methylimidazolium chloride. J. Chem. Phys. 146, 094502 https://doi.org/10.1063/1.4977044.

Ciesielczyk, F., Krysztafkiewicz, Æ.A., 2007. Physicochemical studies on precipitated magnesium silicates, 42, 3831–3840. https://doi.org/10.1007/s10853-006-0464-2.

Ciesielczyk, F., Krysztafkiewicz, A., Jesionowski, T., 2007a. Magnesium silicates – adsorbents of organic compounds, 253, 8435–8442. https://doi.org/10.1016/j.apsusc.2007.04.016.

Ciesielczyk, F., Krysztafkiewicz, Æ.A., Jesionowski, T., 2007b. Adsorptive properties of synthetic magnesium silicates. Physicochem. Probl. Min. Proc. 41, 185–193.

Claverie, M., Dumas, A., Carême, C., Poirier, M., Le Roux, C., Micoud, P., Martin, F., Aymonier, C., 2018. Synthetic talc and talc-like structures: preparation, features and applications. Chem. Eur. J. 24, 519–542. https://doi.org/10.1002/chem.201702763.

Comès, A., Fiorilli, S., Aprile, C., 2020. Multifunctional heterogeneous catalysts highly performing in the conversion of carbon dioxide: mechanistic insights. J. CO2 Utiliz. 37, 213–221. https://doi.org/10.1016/j.jcou.2019.12.008.

Corvo, M.C., Sardinha, J., Menezes, S.C., Einloft, S., Seferin, M., Dupont, J., Casimiro, T., Cabrita, E.J., 2013. Angewandte solvation of carbon dioxide in [C 4 mim][BF 4] and [C 4 mim][PF 6] ionic liquids revealed by high-pressure NMR spectroscopy **. Angew. Chem. Int. Ed. 52, 13024–13027. https://doi.org/10.1002/anie.201305630.

Dias, G., Prado, M.A., Carone, C., Ligabue, R., Dumas, A., Martin, F., Le Roux, C., Micoud, P., Einloft, S., 2015. Synthetic silico-metallic mineral particles (SSMMP) as nanofillers: comparing the effect of different hydrothermal treatments on the PU/SSMMP nanocomposites properties. Polym. Bull. 72, 2991–3006. https://doi.org/10.1007/s00289-015-1449-6.

Dias, G., Prado, M., Carone, C., Ligabue, R., Dumas, A., Le Roux, C., Micoud, P., Martin, F., Einloft, S., 2016. Comparing different synthetic talc as fillers for polyurethane nanocomposites. Macromol. Symp. 367, 136–142. https://doi.org/10.1002/masy.201500141.

Dietemann, M., 2012. Étude de la précipitation du silicate de magnésium amorphe assistée par ultrasons: synthèse, caractérisation et modélisation. Ph.D. thesis. Université de Toulouse, Université Toulouse III - Paul Sabatier, France.

Dinda, S., 2013. Development of solid adsorbent for carbon dioxide capture from flue gas. Sep. Purif. Technol. https://doi.org/10.1016/j.seppur.2013.02.027.

dos Santos, L.M., Bernard, F.L., Polesso, B.B., Pinto, I.S., Frankenberg, C.C., Corvo, M.C., Almeida, P.L., Cabrita, E., Einloft, S., 2020. Designing silica xerogels containing RTIL for CO2 capture and CO2/CH4 separation: Influence of ILs anion, cation and cation side alkyl chain length and ramification. J. Environ. Manag. 268, 1–10. https://doi.org/10.1016/j.jenvman.2020.110340.

Du, T., Liu, L. Ying, Xiao, P., Che, S., Wang, H. Ming, 2014. Preparation of zeolite NaA for CO2 capture from nickel laterite residue. Int. J. Miner. Metall. Mater. 21, 820–825. https://doi.org/10.1007/s12613-014-0976-8.

Duczinski, R., Bernard, F., Rojas, M., Duarte, E., Chaban, V., Vecchia, F.D., Menezes, S., Einloft, S., 2018. Waste derived MCMRH- supported IL for CO2/CH4 separation. J. Nat. Gas Sci. Eng. 54, 54–64. https://doi.org/10.1016/j.jngse.2018.03.028.

Dumas, A., 2013. Élaboration de Nouveaux Procédés de Synthèse et Caractérisation de Talcs Sub-Microniques: De La Recherche Fondamentale Vers Des Applications Industrielles. Ph.D. thesis. Université de Toulouse, Université Toulouse III - Paul Sabatier, France.

Dumas, A., Le Roux, C., Martin, F., Micoud, P., 2013a. Method for preparing a hydrogel comprising silico-metallic mineral particles and hydrogel. In: Patent Application WO2013/093339.

Dumas, A., Martin, F., Ferrage, E., Micoud, P., Le Roux, C., Petit, S., 2013b. Synthetic talc advances: coming closer to nature, added value, and industrial requirements. Appl. Clay Sci. 85, 8–18. https://doi.org/10.1016/j.clay.2013.09.006.

Dumas, A., Martin, F., Le Roux, C., Micoud, P., Petit, S., Ferrage, E., Brendlé, J., Grauby, O., Greenhill-Hooper, M., 2013c. Phyllosilicates synthesis: a way of accessing edges contributions in NMR and FTIR spectroscopies. Example of synthetic talc. Phys. Chem. Miner. 40, 361–373. https://doi.org/10.1007/s00269-013-0577-5.

Dumas, A., Le Roux, C., Martin, F., Micoud, P., 2014a. Method for preparing a composition comprising functionalised silico/germano-metal particles and composition obtained. In: Patent Application WO2014/202920.

Dumas, A., Le Roux, C., Martin, F., Micoud, P., 2014b. Method for preparing a composition comprising functionalised mineral particles and corresponding composition. In: Patent Application WO2014/207397.

Dumas, A., Mizrahi, M., Martin, F., Requejo, F., 2015. Local and Extended-Order Evolution of Synthetic Talc during Hydrothermal Synthesis: Extended X - ray Absorption Fine Structure, X - ray Diffraction, and Fourier Transform Infrared Spectroscopy Studies, 15, pp. 5451–5463. https://doi.org/10.1021/acs.cgd.5b01076.

Espinal, L., Poster, D.L., Wong-Ng, W., Allen, A.J., Green, M.L., 2013. Measurement, standards, and data needs for CO2 capture materials: a critical review. Environ. Sci. Technol. 47, 11960–11975. https://doi.org/10.1021/es402622q.

Fawzy, S., Osman, A.I., Doran, J., Rooney, D.W., 2020. Strategies for mitigation of climate change: a review. Environ. Chem. Lett. 18, 2069–2094. https://doi.org/10.1007/s10311-020-01059-w.

Fuji, K., Hayashi, S., 2005. Hydrothermal syntheses and characterisation of alkylammonium phyllosilicates containing CSiO3 and SiO4 units. Appl. Clay Sci. 29, 235–248. https://doi.org/10.1016/j.clay.2005.01.005.

Fujiki, J., Yamada, H., Yogo, K., 2015. Enhanced adsorption of carbon dioxide on surface-modified mesoporous silica-supported tetraethylenepentamine: Role of surface chemical structure. Microporous Mesoporous Mater. 215, 76–83. https://doi.org/10.1016/j.micromeso.2015.05.037.

Gallégo, J.C., Jaber, M., Miehé-Brendlé, J., Marichal, C., 2008. Synthesis of new lamellar inorganic-organic talc-like hybrids. New J. Chem. 32, 407–412. https://doi.org/10.1039/b713004j.

Gao, H., Liang, Z., Liao, H., Idem, R.O., 2014. Thermal degradation of aqueous DEEA solution at stripper conditions for post-combustion CO2 capture. Chem. Eng. Sci. 135, 330–342. https://doi.org/10.1016/j.ces.2015.02.033.

Grondin, J., Lassègues, J.C., Cavagnat, D., Buffeteau, T., Holomb, R., 2011. Revisited vibrational assignments of imidazolium-based ionic liquids. J. Raman Spectrosc. 42, 733–743. https://doi.org/10.1002/jrs.2754.

Harvey, I., Madani, S.H., Huang, J., Pendleton, P., 2016. Carbon dioxide adsorption by zinc-functionalized ionic liquid impregnated into bio-templated mesoporous silica beads. Chem. Eng. J. 283, 692–702. https://doi.org/10.1016/j.cej.2015.08.006.

Hasib-ur-rahman, M., Siaj, M., Larachi, F., 2010. Chemical Engineering and Processing: Process Intensification Ionic liquids for CO2 capture — Development and Progress, 49, pp. 313–322. https://doi.org/10.1016/j.cep.2010.03.008.

He, Y., Seaton, N.A., 2006. Heats of adsorption and adsorption heterogeneity for methane, ethane, and carbon dioxide in MCM-41. Langmuir 22, 1150–1155. https://doi.org/10.1021/la052237k.

Houshmand, A., Shafeeyan, M.S., Arami-niya, A., Mohd, W., Wan, A., 2013. Anchoring a halogenated amine on the surface of a microporous activated carbon for carbon dioxide capture. J. Taiwan Inst. Chem. Eng. 44, 774–779. https://doi.org/10.1016/j.jtice.2013.01.014.

Kamarudin, K.S.N., Alias, N., 2013. Adsorption performance of MCM-41 impregnated with amine for CO2 removal. Fuel Process. Technol. 106, 332–337. https://doi.org/10.1016/j.fuproc.2012.08.017.

Kinik, F.P., Altintas, C., Balci, V., Koyuturk, B., Uzun, A., Keskin, S., 2016. [BMIM][PF6] incorporation doubles CO2 selectivity of ZIF-8: elucidation of interactions and their consequences on performance. ACS Appl. Mater. Interfaces 8, 30992–31005. https://doi.org/10.1021/acsami.6b11087.

Kloprogge, J.T., 2017. Raman Spectroscopy of Clay Minerals, 1st ed, Infrared and Raman Spectroscopies of Clay Minerals. Elsevier Ltd. https://doi.org/10.1016/B978-0-08-100355-8.00006-0

Kodasma, R., Fermoso, J., Sanna, A., 2019. Li-LSX-zeolite evaluation for post-combustion CO2 capture. Chem. Eng. J. 358, 1351–1362. https://doi.org/10.1016/j.cej.2018.10.063.

Kong, Y., Jiang, G., Fan, M., Shen, X., Cui, S., Russell, A.G., 2014. A new aerogel based CO2 adsorbent developed using a simple sol-gel method along with supercritical drying. Chem. Commun. 50, 12158–12161. https://doi.org/10.1039/c4cc06424k.

Koros, W.J., Paul, D.R., 1976. Design considerations for measurement of gas sorption in polymers by pressure decay. J. Polym. Sci. Polym. Phys. Ed. 14, 1903–1907. https://doi.org/10.1002/pol.1976.180141014.

Li, M., Tian, M., Chen, H., Mahurin, S.M., Wu, Z., Dai, S., 2020. H2O-prompted CO2capture on metal silicates: in situ generated from SBA-15. RSC Adv. 10, 28731–28740. https://doi.org/10.1039/d0ra02736g.

Linneen, N., Pfeffer, R., Lin, Y.S., 2013. CO 2 capture using particulate silica aerogel immobilized with tetraethylenepentamine. Microporous Mesoporous Mater. 176, 123–131. https://doi.org/10.1016/j.micromeso.2013.02.052.

Liu, J., Lin, R., 2013. Structural properties and reactivities of amino-modi fi ed silica fume solid sorbents for low-temperature CO 2 capture. Powder Technol. 241, 188–195. https://doi.org/10.1016/j.powtec.2013.03.022.

Loganathan, S., Ghoshal, A.K., 2017. Amine tethered pore-expanded MCM-41: a promising adsorbent for CO2 capture. Chem. Eng. J. 308, 827–839. https://doi.org/10.1016/j.cej.2016.09.103.

Malherbe, R., Estrella, R., Linares, F., 2010. Study of the interaction between silica surfaces and the carbon dioxide molecule. J. Phys. Chem. C 114 (41), 17773–17787. https://doi.org/10.1021/jp107754g.

Maria, G., Airoldi, C., 2001. New amino-inorganic hybrids from talc silylation and copper adsorption properties, 36, 277–287.

Meléndez-Ortiz, H.I., Perera-Mercado, Y., Mercado-Silva, J.A., Olivares-Maldonado, Y., Castruita, G., García-Cerda, L.A., 2014. Functionalization with amine-containing organosilane of mesoporous silica MCM-41 and MCM-48 obtained at room temperature. Ceram. Int. 40, 9701–9707. https://doi.org/10.1016/j.ceramint.2014.02.051.

Mohamedali, M., Ibrahim, H., Henni, A., 2018. Incorporation of acetate-based ionic liquids into a zeolitic imidazolate framework (ZIF-8) as efficient sorbents for carbon dioxide capture. Chem. Eng. J. 334, 817–828. https://doi.org/10.1016/j.cej.2017.10.104.

Mohamedali, M., Ibrahim, H., Henni, A., 2020. Imidazolium based ionic liquids confined into mesoporous silica MCM-41 and SBA-15 for carbon dioxide capture. Microporous Mesoporous Mater. 294, 109916 https://doi.org/10.1016/j.micromeso.2019.109916.

Mor, S., Manchanda, C.K., Kansal, S.K., Ravindra, K., 2017. Nanosilica extraction from processed agricultural residue using green technology. J. Clean. Prod. 143, 1284–1290. https://doi.org/10.1016/j.jclepro.2016.11.142.

Muldoon, M.J., Aki, S.N.V.K., Anderson, J.L., Dixon, J.K., Brennecke, J.F., 2007. Improving carbon dioxide solubility in ionic liquids. J. Phys. Chem. B 111, 9001–9009. https://doi.org/10.1021/jp071897q.

Nicot, J.P., Duncan, I.J., 2012. Review: Common attributes of hydraulically fractured oil and gas production and CO2 geological sequestration. Greenhouse Gases Sci. Technol. 2, 352–368. https://doi.org/10.1002/ghg.

Nikolaidis, G.N., Kikkinides, E.S., Georgiadis, M.C., 2018. A model-based approach for the evaluation of new zeolite 13X-based adsorbents for the efficient post-combustion CO2 capture using P/VSA processes. Chem. Eng. Res. Des. 131, 362–374. https://doi.org/10.1016/j.cherd.2017.06.016.

Nkinahamira, F., Su, T., Xie, Y., Ma, G., Wang, H., Li, J., 2017. High pressure adsorption of CO 2 on MCM-41 grafted with quaternary ammonium ionic liquids, 326, 831–838. https://doi.org/10.1016/j.cej.2017.05.173.

Nonthanasin, T., Henni, A., Saiwan, C., 2014. Densities and low pressure solubilities of carbon dioxide in five promising ionic liquids. RSC Adv. 4, 7566–7578. https://doi.org/10.1039/c3ra46339g.

Olajire, A.A., 2018. Synthesis chemistry of metal-organic frameworks for CO2 capture and conversion for sustainable energy future. Renew. Sust. Energ. Rev. 92, 570–607. https://doi.org/10.1016/j.rser.2018.04.073.

Ouyang, J., Zheng, C., Gu, W., Zhang, Y., Yang, H., Suib, S.L., 2018. Textural properties determined CO2 capture of tetraethylenepentamine loaded SiO2 nanowires from A-sepiolite. Chem. Eng. J. 337, 342–350. https://doi.org/10.1016/j.cej.2017.12.109.

Paschoal, V.H., Faria, L.F.O., Ribeiro, M.C.C., 2017. Vibrational spectroscopy of ionic liquids. Chem. Rev. 117, 7053–7112. https://doi.org/10.1021/acs.chemrev.6b00461.

Polesso, B.B., Duczinski, R., Bernard, F.L., Ferrari, H.Z., Da Luz, M., Vecchia, F.D., De Menezes, S.M.C., Einloft, S., 2019. Imidazolium-based ionic liquids impregnated in silica and alumina supports for CO2 capture. Mater. Res. 22, 1–10. https://doi.org/10.1590/1980-5373-MR-2018-0810.

Prado, M.A., Dias, G., dos Santos, L.M., Ligabue, R., Poirier, M., Le Roux, C., Micoud, P., Martin, F., Einloft, S., 2020. The influence of Ni/Mg content of synthetic Mg/Ni talc on mechanical and thermal properties of waterborne polyurethane nanocomposites. SN Appl. Sci. 2, 1–13. https://doi.org/10.1007/s42452-020-2852-7.

Ramdin, M., De Loos, T.W., Vlugt, T.J.H., 2012. State-of-the-art of CO 2 capture with ionic liquids. Ind. Eng. Chem. Res. 51, 8149–8177. https://doi.org/10.1021/ie3003705.

Razavi, S.S., Hashemianzadeh, S.M., Karimi, H., 2011. Modeling the adsorptive selectivity of carbon nanotubes for effective separation of CO2/N2 mixtures. J. Mol. Model. 17, 1163–1172. https://doi.org/10.1007/s00894-010-0810-9.

Rimola, A., Costa, D., Sodupe, M., Lambert, J.F., Ugliengo, P., 2013. Silica surface features and their role in the adsorption of biomolecules: Computational modeling and experiments. Chem. Rev. 113, 4216–4313. https://doi.org/10.1021/cr3003054.

Rojas, M., Pacheco, L., Martinez, A., Pradilla, K., Bernard, F., Einloft, S., Carre, L.A., 2017. New Biocomposites Based on castor Oil Polyurethane Foams and Ionic Liquids for CO 2 Capture 452. https://doi.org/10.1016/j.fluid.2017.08.026.

Sabouni, R., Kazemian, H., Rohani, S., 2014. Carbon dioxide capturing technologies: a review focusing on metal organic framework materials (MOFs), 21, 5427–5449. https://doi.org/10.1007/s11356-013-2406-2.

Sanz, R., Calleja, G., Arencibia, A., Sanz-Pérez, E.S., 2010. CO 2 adsorption on branched polyethyleneimine-impregnated mesoporous silica SBA-15. Appl. Surf. Sci. 256, 5323–5328. https://doi.org/10.1016/j.apsusc.2009.12.070.

Schroeder, P., 2002. Infrared spectroscopy in clay science. CMS Workshop Lectures 11, 181–206.

Sexton, A.J., Rochelle, G.T., 2011. Reaction Products from the Oxidative Degradation of Monoethanolamine, 50, pp. 667–673. https://doi.org/10.1021/ie901053s.

Seyed, J.S., Nazemzadeh, H., 2017. Nanoparticles as an efficient catalyst for the preparation of propargylamines. Res. Chem. Intermed. 43, 7375–7386. https://doi.org/10.1007/s11164-017-3081-6.

Simon, N., Zanatta, M., Neumann, J., Girard, A., Marin, G., Stassen, H., Dupont, J., 2018. Cation À Anion À CO 2 Interactions in Imidazolium-based ionic liquid sorbents. ChemPhysChem 19, 2879–2884. https://doi.org/10.1002/cphc.201800751.

Talaty, E.R., Raja, S., Storhaug, V.J., Do, A., Carper, W.R., 2004. Raman and infrared spectra and ab initio calculations of C 2–4 MIM imidazolium hexafluorophosphate ionic liquids. Phys. Chem. B 108, 13177–13184. https://doi.org/10.1021/jp040199s.

Wang, X., Chen, L., Guo, Q., 2015. Development of hybrid amine-functionalized MCM-41 sorbents for CO2capture. Chem. Eng. J. 260, 573–581. https://doi.org/10.1016/j.cej.2014.08.107.

Wang, Y., Zhao, L., Otto, A., Robinius, M., Stolten, D., 2017. A review of post-combustion CO2 Capture technologies from coal-fired power plants. Energy Procedia 114, 650–665. https://doi.org/10.1016/j.egypro.2017.03.1209.

Xiao, M., Liu, H., Gao, H., Liang, Z., 2018. CO2 absorption with aqueous tertiary amine solutions: equilibrium solubility and thermodynamic modeling. J. Chem. Thermodyn. 122, 170–182. https://doi.org/10.1016/j.jct.2018.03.020.

Younas, M., Rezakazemi, M., Daud, M., Wazir, M.B., Ahmad, S., Ullah, N., Inamuddin, Ramakrishna S., 2020. Recent progress and remaining challenges in post-combustion CO2 capture using metal-organic frameworks (MOFs). Prog. Energy Combust. Sci. 80, 100849 https://doi.org/10.1016/j.pecs.2020.100849.

Yu, J., Balbuena, P.B., 2013. Water effects on postcombustion Co2 capture in Mg-MOF-74. J. Phys. Chem. C 117, 3383–3388. https://doi.org/10.1021/jp311118x.

Yu, C.H., Huang, C.H., Tan, C.S., 2012. A review of CO2 capture by absorption and adsorption. Aerosol Air Qual. Res. 12, 745–769. https://doi.org/10.4209/aaqr.2012.05.0132.

Zhang, Z., Xian, S., Xi, H., Wang, H., Li, Z., 2011. Improvement of CO2 adsorption on ZIF-8 crystals modified by enhancing basicity of surface. Chem. Eng. Sci. 66, 4878–4888. https://doi.org/10.1016/j.ces.2011.06.051.

Zhang, L., Wang, X., Fujii, M., Yang, L., Song, C., 2017. CO2 capture over molecular basket sorbents: Effects of SiO2 supports and PEG additive. J. Energy Chem. 26, 1030–1038. https://doi.org/10.1016/j.jechem.2017.09.002.

Zhang, Y., Chen, M., Li, G., Shi, C., Wang, B., Ling, Z., 2020. Results in Materials Exfoliated vermiculite nanosheets supporting tetraethylenepentamine for CO 2 capture. Results in Materials 7, 100102. https://doi.org/10.1016/j.rinma.2020.100102.

Zhu, J., He, B., Huang, J., Li, C., Ren, T., 2018. Effect of immobilization methods and the pore structure on CO2 separation performance in silica-supported ionic liquids. Microporous Mesoporous Mater. 260, 190–200. https://doi.org/10.1016/j.micromeso.2017.10.035.